

Large-Scale Discrete Fourier Transform on TPUs

Tianjian Lu, Yi-Fan Chen, Blake Hechtman, Tao Wang, and John Anderson

Abstract—In this work, we present a parallel algorithm for large-scale discrete Fourier transform (DFT) on Tensor Processing Unit (TPU) clusters. The algorithm is implemented in TensorFlow because of its rich set of functionalities for scientific computing and simplicity in realizing parallel computing algorithms. The DFT formulation is based on matrix multiplications between the input data and the Vandermonde matrix. This formulation takes full advantage of TPU’s strength in matrix multiplications and allows nonuniformly sampled input data without modifying the implementation. For the parallel computing, both the input data and the Vandermonde matrix are partitioned and distributed across TPU cores. Through the data decomposition, the matrix multiplications are kept local within TPU cores and can be performed completely in parallel. The communication among TPU cores is achieved through the one-shuffle scheme, with which sending and receiving data takes place simultaneously between two neighboring cores and along the same direction on the interconnect network. The one-shuffle scheme is designed for the interconnect topology of TPU clusters, requiring minimal communication time among TPU cores. Numerical examples are used to demonstrate the high parallel efficiency of the large-scale DFT on TPUs.

Index Terms—Discrete Fourier transform, Hardware accelerator, Parallel computing, TensorFlow, Tensor processing unit

I. INTRODUCTION

The discrete Fourier transform (DFT) is critical in many scientific and engineering applications, including time series and waveform analyses, convolution and correlation computations, solutions to partial differential equations, density function theory in first-principle calculations, spectrum analyzer, synthetic aperture radar, computed tomography, magnetic resonance imaging, and derivatives pricing [1]–[4]. However, the computation efficiency of DFT is often the formidable bottleneck in handling large-scale problems due to the large data size and real-time-processing requirement [5], [6]. In general, efforts on enhancing the computation efficiency of DFT fall into two categories: seeking fast algorithms and adapting the algorithms to parallel computing. One breakthrough of the fast-algorithm category is the Cooley-Tukey algorithm [7], also known as the fast Fourier transform (FFT), which reduces the complexity of N -point DFT from $O(N^2)$ to $O(N \log N)$. The Cooley-Tukey algorithm assuming that the number of data is a power of two is known as the Radix-2 algorithm and followed by Mixed-Radix [3] and Split-Radix [8] algorithms. In addition to the fast algorithms, the performance of parallel computing has been steadily driving the efficiency enhancement of DFT computation: the first implementation of the FFT algorithm was realized on ILLIAC IV parallel computer [9], [10]; over the years, the DFT computation has been adapted to both shared-

memory [11], [12] and distributed-memory architectures [13]–[17].

The advancement of hardware accelerators has enabled massive parallelization for DFT computation. One such example is deploying the FFT computation on manycore processors [18]. Another example is implementing the FFT algorithm on clusters of graphics processing units (GPUs) [19]. A GPU cluster contains a number of nodes (machines) and within each node, GPUs are connected through PCIe, a high-speed serial interface. The Cooley-Tukey algorithm and its variants often require a large number of memory accesses per arithmetic operation such that the bandwidth limitation of PCIe becomes the computation bottleneck of the overall performance of FFT on GPU clusters. Prior to the recent development of novel high-speed interconnects such as NVLink [20], [21], many efforts related to the GPU-accelerated DFT computation are spent on minimizing the PCIe transfer time [3], [22]. It is worth mentioning that the route of algorithm-hardware co-design has also been taken with Field Programmable Gate Arrays (FPGAs) to optimize the configurations of a customized hardware accelerator for high-performance computing of DFT [23]–[25].

The recent success of machine learning (ML), or deep learning (DL) in particular, has spurred a new wave of hardware accelerators. In many ML applications, it becomes increasingly challenging to balance the performance-cost-energy of processors with the growth of data. Domain-specific hardware is considered as a promising approach to achieve so [26]. One example of the domain-specific hardware is Google’s Tensor Processing Unit (TPU) [27]. As a reference, TPU v3 provides 480 teraflops and 128 GiB high-bandwidth memory (HBM) [28]. In witnessing how DFT computation benefits from the development of hardware accelerators, it is tempting to ask whether TPU can empower the large-scale DFT computation. It is plausible with the following four reasons. First, TPU is a ML application-specific integrated circuit (ASIC), devised for neural networks (NNs). NNs require massive amounts of multiplications and additions between the data and parameters and TPU can handle these computations in terms of matrix multiplications in a very efficient manner [29]. Similarly, DFT can also be formulated as matrix multiplications between the input data and the Vandermonde matrix. Second, TPU chips are connected directly to each other with dedicated high-speed interconnects of very low latency and without going through a host CPU or utilizing networking resources. Therefore, the large-scale DFT computation can be distributed among multiple TPUs with minimal communication time and hence very high parallel efficiency. Third, the large capacity of the in-package memory of TPU makes it possible to handle large-scale DFT efficiently. Fourth, TPU is programmable with software front ends such as TensorFlow [30] and PyTorch [31].

The authors are with Google Research, 1600 Amphitheatre Pkwy, Mountain View, CA 94043, USA, e-mail: {tianjianlu, yifanchen, blakehechtman, wangtao, janders}@google.com.

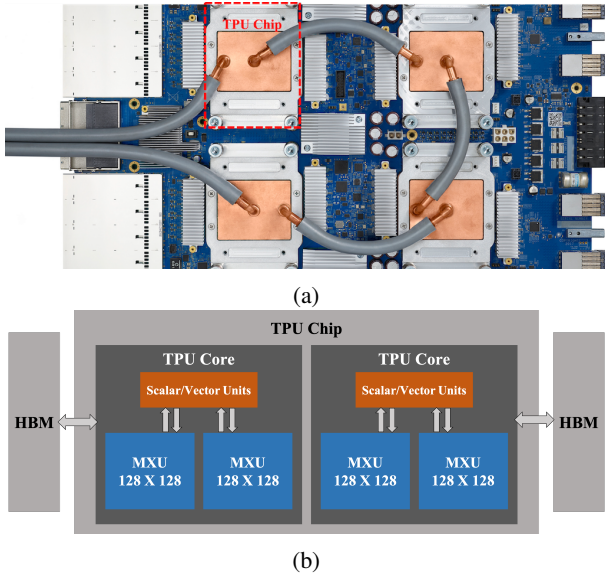


Fig. 1: (a) TPU v3 has four chips on the same board and (b) each chip contains two cores.

TensorFlow offers a rich set of functionalities for scientific computing and the TensorFlow TPU programming stack can express the parallel computing algorithms with simple and easy-to-understand code without sacrificing the performance, both of which make it straightforward to implement the parallel computing of DFT on TPUs. In fact, all the aforementioned four reasons have been verified in the high-performance Monte Carlo simulations on TPUs [32], [33].

In this work, we present the implementation of large-scale DFT on TPUs. The implementation is in TensorFlow. The DFT formulation is based on matrix multiplications between the input data and the Vandermonde matrix with the complexity of $O(N^2)$ for N -point DFT. This formulation takes full advantage of TPU’s strength in matrix multiplications and allows nonuniformly sampled input data without modifying the implementation. The nonuniform DFT has important applications in signal processing, medical imaging, numerical solutions of partial differential equations, and machine learning [34]–[37]. For the parallel computing, both the input data and the Vandermonde matrix are partitioned and distributed across TPU cores. Through the data decomposition, the matrix multiplications are kept local within TPU cores and can be performed completely in parallel. The communication among TPU cores is achieved through the one-shuffle scheme, with which sending and receiving data takes place simultaneously between two neighboring cores and along the same direction on the interconnect network. The one-shuffle scheme is designed for the interconnect topology of TPU clusters, which requires minimal communication time among TPU cores. Numerical examples are used to demonstrate the high parallel efficiency of the large-scale DFT on TPUs.

II. TPU SYSTEM ARCHITECTURE

Understanding the advantages of deploying the large-scale DFT computation on TPUs cannot be separated from the

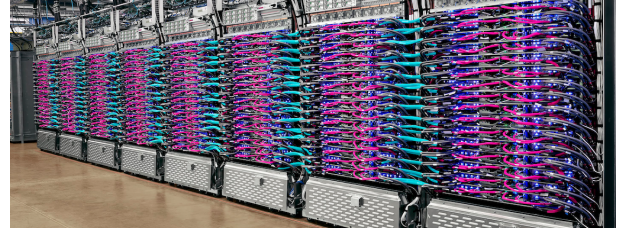


Fig. 2: TPU v3 Pod in a data center.

knowledge of TPU system architecture. In this section, we provide an overview of the TPU system architecture on both the hardware and software components.

A. Hardware architecture

Figure 1 shows one TPU board or unit: there are four TPU chips on the same board; each chip has two cores; and each core contains the scalar, vector, and matrix units (MXU). MXU provides the bulk of the compute power of a TPU chip. Structured as a 128×128 systolic array, MXU can handle 16 K multiply-accumulate (MAC) operations in one single clock cycle. Both the inputs and outputs of MXU are float32, whereas MXU performs MAC operations with bfloat16 [38]. However, one float32 number can be decomposed into multiple bfloat16 numbers and with appropriate accumulations, high-precision MAC operation can be achieved [39]. The DFT computation in this work leverages the strategy of decomposition and accumulation and achieves the precision of float32. As shown in Fig. 1(b), each TPU core has 16 GiB high-bandwidth memory (HBM). The large capacity of in-package memory makes it possible to solve large-scale problems in a highly efficient manner. TPU is designed as coprocessor on the I/O bus: each board shown in Fig. 1(a) is paired with one host server consisting of CPU, RAM, and hard disk; TPU executes the instructions sent from CPU on the host server through PCIe.

In a Pod configuration, TPU chips are connected through dedicated high-speed interconnects of very low latency. Figure 2 shows a TPU v3 Pod in a data center where a total number of 2048 cores are connected to each other. The interconnect topology is a two-dimensional (2D) toroidal mesh with each chip connected to its four nearest neighbors such that the communication takes place in four directions. As the interconnects are on the device, the communication among TPU cores does not go through a host CPU or any networking resource. In order to achieve a high parallel efficiency, the communication time needs to be minimized, which further requires designing the communication strategy in accordance with the TPU interconnect topology. The load balancing and the corresponding one-shuffle communication schemes employed in the DFT computation are explained in the following section.

B. Software architecture

We program TPUs through TensorFlow. It consists of four steps to run a program on TPUs, namely, generating a computational graph, preparing the graph, lowering to high-level

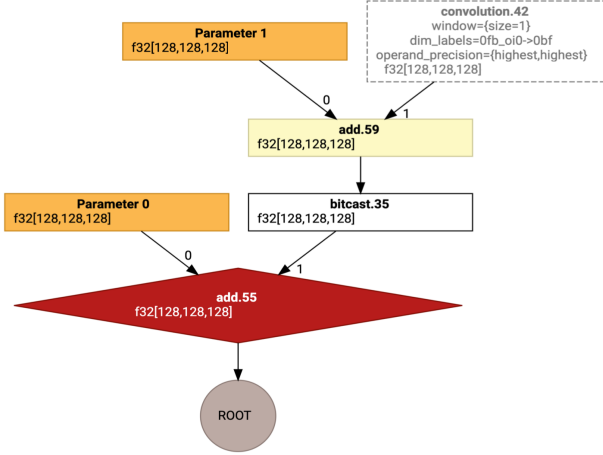


Fig. 3: A computation graph of TensorFlow operations.

optimizer (HLO) operations, and lowering to low-level optimizer (LLO) operations. First, a TensorFlow client converts the TensorFlow operations into a computational graph. A sample computation graph performing addition and convolution operations is shown in Fig. 3. The TensorFlow client sends the graph to a TensorFlow server. Second, the TensorFlow server partitions the computational graph into portions that run on TPU and CPU, respectively. If multiple TPUs are to be employed, the graph is marked for replication. Third, the TensorFlow server compiles the sub-graph that runs on TPUs into a HLO program and invokes the accelerated linear algebra (XLA) compiler. Last, the XLA compiler takes in the HLO program and converts it into a LLO program, which is effectively the assembly code for TPUs. Both the generation and compilation of the computational graph occur on the host server. The compiled LLO code is loaded onto TPUs for execution from the host server through PCIe.

The memory usage of a TPU is determined at compile time. Because both the hardware structure of MXU and the memory subsystem on a TPU core prefer certain shapes of a tensor variable for an operation, XLA performs the data layout transformations in order for the hardware to efficiently process the operation. If a tensor variable does not align with the preferred shape, XLA pads zeros along one dimension to make it a multiple of eight and the other dimension to a multiple of 128. Zero padding under-utilizes the TPU core and leads to sub-optimal performance, which should be taken into account in load balancing for the parallel computing of DFT on TPUs.

III. DFT FORMULATION

In this section, we formulate the DFT as matrix multiplications through the Kronecker product [40] between the input data and the Vandermonde matrix. This formulation fully utilizes the strength of TPU, in particular, MXU in matrix multiplications. In addition, it can be applied to nonuniformly sampled data [34], [35] without additional modification to the implementation.

A. Matrix formulation

The general form of DFT is defined as

$$X_k \triangleq X(z_k) = \sum_{n=0}^{N-1} x_n z_k^{-n}, \quad (1)$$

where \triangleq denotes “defined to be”, x_n represents the input, and $\{z_k\}_{k=0}^{N-1}$ are N distinctly and arbitrarily sampled points on the z -plane. Equation (1) can be rewritten into the matrix form

$$\{X\} = [V] \{x\}, \quad (2)$$

where

$$\begin{aligned} \{X\} &= (X(z_0), X(z_1), \dots, X(z_{N-1}))^T, \\ \{x\} &= (x_0, x_1, \dots, x_{N-1})^T, \end{aligned}$$

and

$$[V] = \begin{pmatrix} 1 & z_0^{-1} & z_0^{-2} & \dots & z_0^{-(N-1)} \\ 1 & z_1^{-1} & z_1^{-2} & \dots & z_1^{-(N-1)} \\ \vdots & \vdots & \vdots & \ddots & \vdots \\ 1 & z_{N-1}^{-1} & z_{N-1}^{-2} & \dots & z_{N-1}^{-(N-1)} \end{pmatrix}. \quad (3)$$

Note that $[V]$ is the Vandermonde matrix of dimension $N \times N$. Computing the inverse DFT is equivalent to solving the linear system in Equation (2). In the situation when $\{z_k\}_{k=0}^{N-1}$ are uniformly sampled on the z -plane, the Vandermonde matrix $[V]$ becomes unitary and contains the roots of unity.

The general form of a 2D DFT can be written as

$$X(z_{1k}, z_{2k}) = \sum_{n_1=0}^{N_1-1} \sum_{n_2=0}^{N_2-1} x(n_1, n_2) z_{1k}^{-n_1} z_{2k}^{-n_2}, \quad (4)$$

where $[x]$ has the dimension of $N_1 \times N_2$ and $\{(z_{1k}, z_{2k})\}_{k=0}^{N_1 N_2 - 1}$ represents the set of distinctly and arbitrarily sampled points in (z_1, z_2) space. It is worth mentioning that the sampling with (z_{1k}, z_{2k}) has to ensure the existence of the inverse DFT. If the sampling is performed on rectangular grids, Equation (4) can be rewritten into the matrix form as

$$[X] = [V_1] [x] [V_2]^T, \quad (5)$$

where

$$[X] = \begin{pmatrix} X(z_{10}, z_{20}) & X(z_{10}, z_{21}) & \dots & X(z_{10}, z_{2, N_2-1}) \\ X(z_{11}, z_{20}) & X(z_{11}, z_{21}) & \dots & X(z_{11}, z_{2, N_2-1}) \\ \vdots & \vdots & \ddots & \vdots \\ X(z_{1, N_1-1}, z_{20}) & X(z_{1, N_1-1}, z_{21}) & \dots & X(z_{1, N_1-1}, z_{2, N_2-1}) \end{pmatrix}, \quad (6)$$

$$[x] = \begin{pmatrix} x(0,0) & x(0,1) & \dots & x(0, N_2-1) \\ x(1,0) & x(1,1) & \dots & x(1, N_2-1) \\ \vdots & \vdots & \ddots & \vdots \\ x(N_1-1,0) & x(N_1-1,1) & \dots & x(N_1-1, N_2-1) \end{pmatrix}, \quad (7)$$

$$[V_1] = \begin{pmatrix} 1 & z_{10}^{-1} & z_{10}^{-2} & \dots & z_{10}^{-(N_1-1)} \\ 1 & z_{11}^{-1} & z_{11}^{-2} & \dots & z_{11}^{-(N_1-1)} \\ \vdots & \vdots & \vdots & \ddots & \vdots \\ 1 & z_{1, N_1-1}^{-1} & z_{1, N_1-1}^{-2} & \dots & z_{1, N_1-1}^{-(N_1-1)} \end{pmatrix}, \quad (8)$$

and

$$[V_2] = \begin{pmatrix} 1 & z_{20}^{-1} & z_{20}^{-2} & \cdots & z_{20}^{-(N_2-1)} \\ 1 & z_{21}^{-1} & z_{21}^{-2} & \cdots & z_{21}^{-(N_2-1)} \\ \vdots & \vdots & \vdots & \ddots & \vdots \\ 1 & z_{2,N_2-1}^{-1} & z_{2,N_2-1}^{-2} & \cdots & z_{2,N_2-1}^{-(N_2-1)} \end{pmatrix}. \quad (9)$$

Note that both $[V_1]$ and $[V_2]$ are Vandermonde matrices of dimensions $N_1 \times N_1$ and $N_2 \times N_2$, respectively. One can further lump $[x]$ into a vector such that Equation (5) can be written into the same matrix form as Equation (2), in which $[V]$ for the 2D DFT is expressed as

$$[V] = [V_1] \otimes [V_2], \quad (10)$$

where \otimes denotes the Kronecker product [40].

Similarly, the three-dimensional (3D) DFT defined by

$$X(z_{1k}, z_{2k}, z_{3k}) = \sum_{n_1=0}^{N_1-1} \sum_{n_2=0}^{N_2-1} \sum_{n_3=0}^{N_3-1} x(n_1, n_2, n_3) z_{1k}^{-n_1} z_{2k}^{-n_2} z_{3k}^{-n_3} \quad (11)$$

can be rewritten into the matrix form as

$$\{X\} = [V_1] \otimes [V_2] \otimes [V_3] \{x\}, \quad (12)$$

where

$$[V_j] = \begin{pmatrix} 1 & z_{j0}^{-1} & z_{j0}^{-2} & \cdots & z_{j0}^{-(N_j-1)} \\ 1 & z_{j1}^{-1} & z_{j1}^{-2} & \cdots & z_{j1}^{-(N_j-1)} \\ \vdots & \vdots & \vdots & \ddots & \vdots \\ 1 & z_{j,N_j-1}^{-1} & z_{j,N_j-1}^{-2} & \cdots & z_{j,N_j-1}^{-(N_j-1)} \end{pmatrix}, \quad (13)$$

$j \in \{1, 2, 3\}$.

For the 3D DFT defined in Equation (12), the sampling is performed on rectangular grids in (z_1, z_2, z_3) space and the Vandermonde matrix $[V_3]$ has the dimension of $N_3 \times N_3$. It can be seen that the Kronecker product bridges the gap between the matrix and tensor operations, through which the contraction between a rank-2 tensor and another rank-3 tensor in the 3D DFT can be formulated as matrix multiplications. The DFT formulation with the Kronecker product can be easily extended to higher dimensions.

IV. PARALLEL IMPLEMENTATION ON TPUS

In this section, we take the 3D DFT as an example to illustrate the data decomposition and the corresponding one-shuffle scheme in the parallel computing of DFT on TPUs.

Data decomposition is applied to the input data along all three dimensions. The decomposition is based on a TPU computation shape (P_1, P_2, P_3) where P_1 , P_2 , and P_3 denote the number of TPU cores along the first, the second, and the third dimension, respectively. Given the TPU computation shape (P_1, P_2, P_3) and the input data of dimension $N_1 \times N_2 \times N_3$ and after the data decomposition, each TPU core contains a data block of dimension $\frac{N_1}{P_1} \times \frac{N_2}{P_2} \times \frac{N_3}{P_3}$ as shown in Fig. 4(a). The partition of the Vandermonde matrix is one-way and along the frequency domain. As shown in Fig. 4(b), each core has a slice of the Vandermonde matrix with dimension $\frac{N_i}{P_i} \times N_i$, $i = 1, 2, 3$.

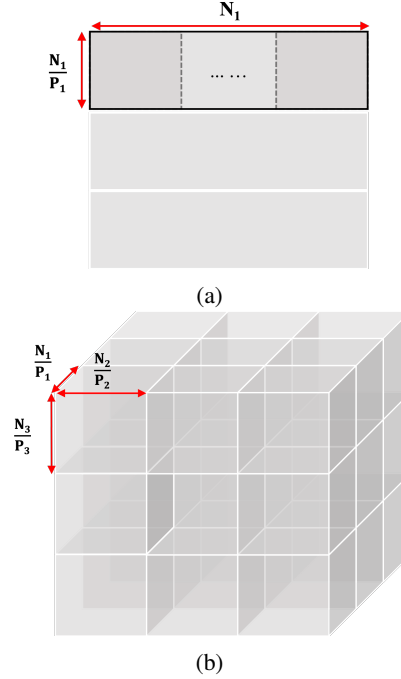


Fig. 4: Through the data decomposition with the TPU computation shape (P_1, P_2, P_3) , each TPU core contains (a) the Vandermonde matrix of dimension $\frac{N_i}{P_i} \times N_i$, $i = 1, 2, 3$ and (b) the block of input data of dimension $\frac{N_1}{P_1} \times \frac{N_2}{P_2} \times \frac{N_3}{P_3}$ for 3D DFT.

Two major operations are employed in the implementation: the tensor contraction between the Vandermonde matrix and the input data; and the communication among TPU cores to send and receive the block of input data. The tensor contraction is based on `einsum` and the communication among TPU cores is with `collective_permute` through the one-shuffle scheme.

Figure 5 illustrates the one-shuffle scheme. We use c_0 , c_1 , and c_2 to denote three adjacent TPU cores, the operations on which are highlighted with three different colors accordingly as shown in Fig. 5. After the data decomposition, core c_0 contains a block of the input data x_{01} and a slice of the Vandermonde matrix $[V_{00}, V_{01}, V_{02}]$, core c_1 contains x_{11} and $[V_{10}, V_{11}, V_{12}]$, and core c_2 contains x_{21} and $[V_{20}, V_{21}, V_{22}]$. With three `einsum` and two `collective_permute` operations, one obtains the partial DFT written as $V_{00} \cdot x_{01} + V_{01} \cdot x_{11} + V_{02} \cdot x_{21}$ on core c_0 , where \cdot represents the tensor contraction. The steps taken by the partial DFT computation along one dimension are as follows:

1. apply `einsum` to compute $V_{00} \cdot x_{01}$ on core c_0 , $V_{11} \cdot x_{11}$ on core c_1 , and $V_{22} \cdot x_{21}$ on core c_2 as shown in Fig. 5(a);
2. apply `collective_permute` to shuffle the input between neighboring TPU cores with source-target pairs (c_1, c_0) , (c_2, c_1) , and (c_0, c_2) in the form of (source, target) such that core c_0 contains x_{11} , core c_1 contains x_{21} , and core c_2 contains x_{01} as shown in Fig. 5(b);

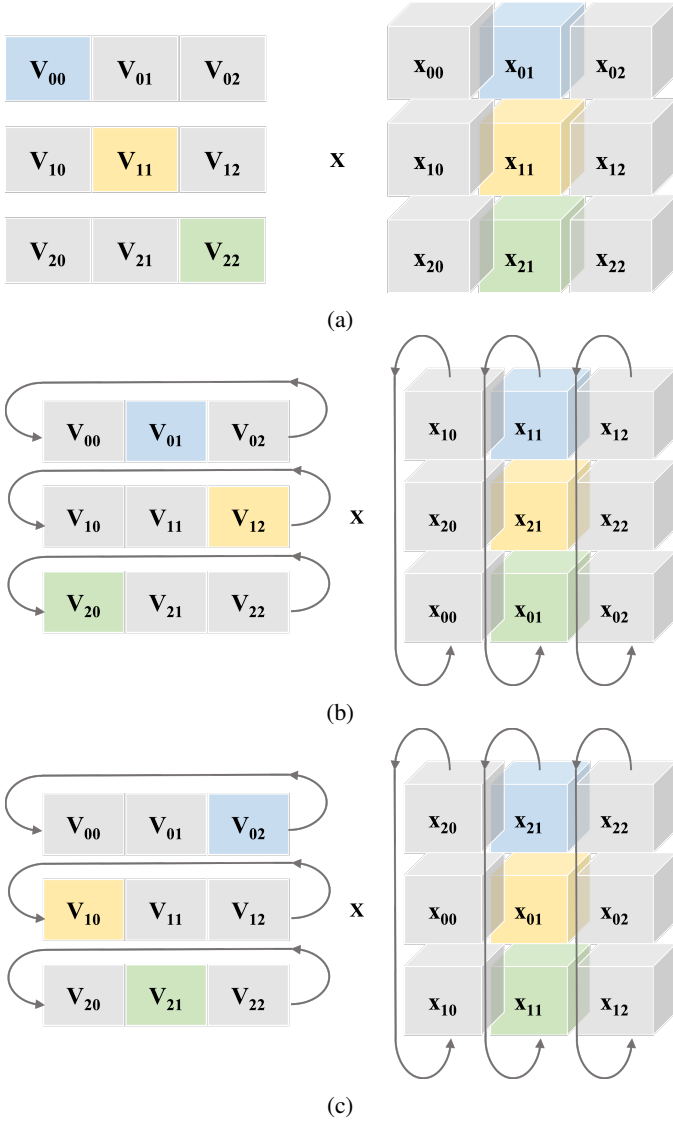


Fig. 5: The one-shuffle scheme is illustrated with the example of the DFT along one dimension in the 3D case. We use c_0 , c_1 , and c_2 to denote three adjacent cores, the operations on which are highlighted with blue, yellow, and green, respectively. The data decomposition results in the block of the input data x_{01} and the slice of the Vandermonde matrix $[V_{00}, V_{01}, V_{02}]$ on core c_0 , x_{11} and $[V_{10}, V_{11}, V_{12}]$ on core c_1 , and x_{21} and $[V_{20}, V_{21}, V_{22}]$ on core c_2 . The steps involved in the one-shuffle scheme are: (a) computing $V_{00} \cdot x_{01}$ on core c_0 , $V_{11} \cdot x_{11}$ on core c_1 , and $V_{22} \cdot x_{21}$ on core c_2 with \cdot representing the operation of tensor contraction; (b) collectively permuting the inputs between two neighboring cores such that x_{11} on core c_0 , x_{21} on core c_1 , and x_{01} on core c_2 and computing $V_{01} \cdot x_{11}$ on core c_0 , $V_{12} \cdot x_{21}$ on core c_1 , and $V_{20} \cdot x_{01}$ on core c_2 ; (c) collectively permuting the inputs such that x_{21} on core c_0 , x_{01} on core c_1 , and x_{11} on core c_2 and computing $V_{02} \cdot x_{21}$ on core c_0 , $V_{10} \cdot x_{01}$ on core c_1 , and $V_{21} \cdot x_{11}$ on core c_2 . The `collective_permute` operation in shuffling the input between neighboring TPU cores is with source-target pairs (c_1, c_0) , (c_2, c_1) , and (c_0, c_2) in the form of (source, target).

3. apply `einsum` to compute $V_{01} \cdot x_{11}$ on core c_0 , $V_{12} \cdot x_{21}$ on core c_1 , and $V_{20} \cdot x_{01}$ on core c_2 and add the results from step 1;
4. apply `collective_permute` with source-target pairs (c_1, c_0) , (c_2, c_1) , (c_0, c_2) , after which core c_0 contains x_{21} , core c_1 contains x_{01} , and core c_2 contains x_{11} as shown in Fig. 5(c);
5. apply `einsum` to compute $V_{02} \cdot x_{21}$ on core c_0 , $V_{10} \cdot x_{01}$ on core c_1 , and $V_{21} \cdot x_{11}$ on core c_2 and add the results from step 3.

The DFT computations along the other two dimensions in the 3D case follow similar steps.

With the one-shuffle scheme, sending and receiving data takes place simultaneously between two neighboring cores and along the same direction on the 2D toroidal network. The one-shuffle scheme best utilizes the topology of the interconnect and hence its bandwidth. Together with the high-speed and low-latency nature of the interconnects, the one-shuffle scheme requires minimal communication time. Besides, all tensor contractions remain local within individual TPU cores, which are computed completely in parallel. Therefore, the proposed implementation of DFT on TPUs can achieve very high parallel efficiency.

V. PARALLEL EFFICIENCY ANALYSIS

In this section, numerical examples are provided to demonstrate the parallel efficiency of DFT on TPUs for both the 2D and 3D cases. The strong scaling is adopted in the parallel efficiency analysis, in which the problem size is kept the same as proportionally more TPU cores are employed.

A. 2D DFT

Figure 6 shows the computation time of the 2D DFT with up to 128 TPU cores on an example of dimension 8192×8192 . It can be seen from Fig. 6 that a near-linear scaling of the computation time with respect to the number of TPU cores is achieved. As a reference, the ideal computation time is also provided in Fig. 6, which is defined by

$$\text{ideal time} = \frac{2 \times T_2}{N_{\text{core}}}, \quad (14)$$

where T_2 denotes the total computation time with two TPU cores and N_{core} is the total number of TPU cores being used. As mentioned in the parallel implementation, the total computation time consists of two parts: the time of matrix multiplications, or `einsum` to be specific, and the communication time of sending and receiving the block of input data across TPU cores. It can be seen from Fig. 6 that the time of matrix multiplications scales linearly with respect to the total number of TPU cores. This is because the matrix multiplications are kept completely local within individual cores. The total computation time of the 2D DFT scales approximately linearly with respect to the number of TPU cores, with the gap between the total and the ideal computation time arising from the communication among TPU cores.

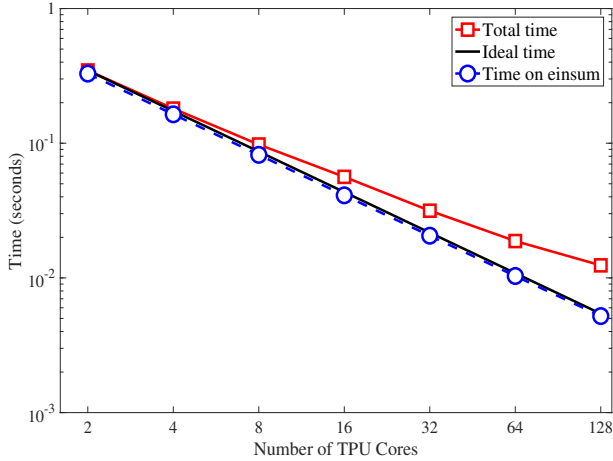


Fig. 6: The computation time of the 2D DFT with up to 128 TPU cores on an example of dimension 8192×8192 .

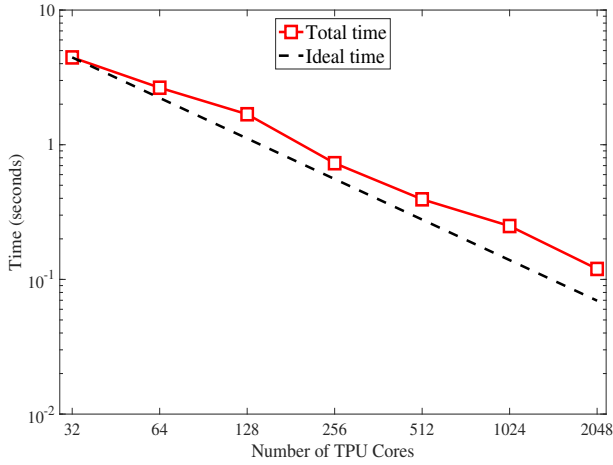


Fig. 7: The computation time of the 3D DFT with up to 2048 TPU cores on an example of dimension $2048 \times 2048 \times 2048$.

B. 3D DFT

The parallel efficiency of the 3D DFT is demonstrated through an example of dimension $2048 \times 2048 \times 2048$. Similar to the 2D case, the problem size is also fixed as proportionally more TPU cores are employed. The total computation time is depicted in Fig. 7. As a reference, the ideal computation time is provided in Fig. 7, which is defined by

$$\text{ideal time} = \frac{32 \times T_{32}}{N_{\text{core}}}, \quad (15)$$

where T_{32} denotes the total computation time with 32 TPU cores. It can be seen from Fig. 7 that the total computation time scales approximately linearly with respect to the number of TPU cores.

The gap between the total and the ideal computation time in the 3D case also results from the communication among TPU cores. As mentioned in the parallel implementation, the data decomposition is applied to the input data along all the three dimensions with a TPU computation shape. The computation shape in this example has the form of $(4, 4, n_2)$ with four TPU cores along the first dimension, four along

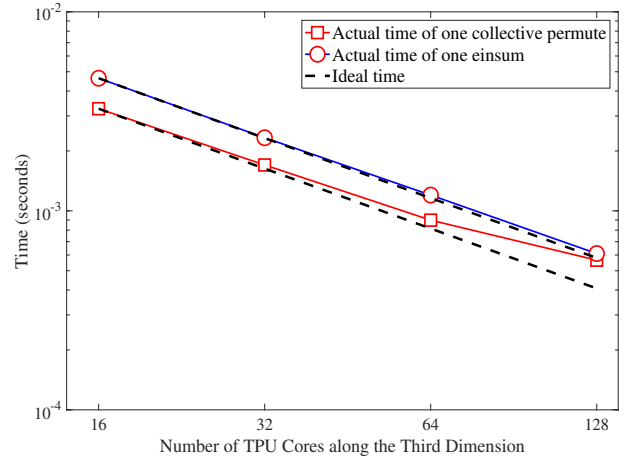


Fig. 8: The computation time of one single operation of `collective_permute` and `einsum`, respectively, in the 3D DFT along the third dimension with respect to the number of TPU cores.

TABLE I: Computation time of the 3D DFT on a full TPU Pod with 2048 TPU cores.

	Problem size	Time (seconds)
1	$8192 \times 8192 \times 8192$	12.66
2	$4096 \times 4096 \times 4096$	1.07
3	$2048 \times 2048 \times 2048$	0.11
4	$1024 \times 1024 \times 1024$	0.02

the second dimension, and n_2 along the third dimension. It is indeed the number of TPU cores along the third dimension that varies in Fig. 7. For example, the computation shapes $(4, 4, 16)$ and $(4, 4, 32)$ are corresponding to 256 and 512 TPU cores, respectively. As the number of TPU cores along the third dimension doubles itself, the size of the input data contained on each core is reduced by half. As a result, the computation time associated with a single operation of `collective_permute` or `einsum` is also reduced by half, which is shown in Fig. 8. However, as more cores are being used, the total number of `collective_permute` operations increases. For example, it requires a total number of 31 `collective_permute` operations in the Fourier transform along the third dimension in the case of 512 TPU cores or with the TPU computation shape $(4, 4, 32)$, whereas only 15 `collective_permute` operations are required in the case of 256 TPU cores or with the TPU computation shape $(4, 4, 16)$. It can be seen that even though the time associated with one single `collective_permute` operation decreases when more TPU cores are used, the total communication time for the DFT along the third dimension does not change. This explains the gap between the total and the ideal computation time in Fig. 7.

In addition to the strong scaling analysis, the computation time of a few 3D DFT examples on a full TPU Pod with 2048 cores is provided in Table I. As the problem size increases

from $2048 \times 2048 \times 2048$ to $4096 \times 4096 \times 4096$, the computation time increases 9.7 times. Similarly, the computation time increases 11.8 times when the problem size increases from $4096 \times 4096 \times 4096$ to $8192 \times 8192 \times 8192$.

VI. CONCLUSION AND DISCUSSION

In this work, we proposed the parallel implementation of DFT on TPUs. Through the implementation, TPU—the domain-specific hardware accelerator for machine learning applications—is employed in the parallel computing of large-scale DFT. The formulation of the DFT is through the Kronecker product and based on matrix multiplications between the input data and the Vandemonde matrix. There are two major advantages associated with this formulation: first, it takes full advantage of TPU’s strength in matrix multiplications; second, it applies to nonuniformly sampled input data without additional modification to the implementation. In the parallel implementation, data decomposition is applied to both the input data and the Vandermonde matrix. Through the data decomposition, the matrix multiplications are kept local within individual TPU cores and performed completely in parallel. As for the communication among TPU cores, the one-shuffle scheme is designed for the TPU interconnect topology, with which sending and receiving data takes place simultaneously between two neighboring cores and along the same direction on the interconnect network. The one-shuffle scheme requires minimal communication time among TPU cores and achieves very high parallel efficiency. Numerical examples of both 2D and 3D are used to demonstrate the high parallel efficiency of the DFT on TPUs. The implementation of DFT on TPUs is with TensorFlow owing to its rich set of functionalities for scientific computing and simplicity in expressing the parallel computing algorithms.

With the demonstrated computation efficiency, the large-scale DFT on TPUs opens an array of opportunities for scientific computing. As a future work, the DFT formulation in this paper can be combined with the Cooley-Tukey algorithm in a way that the overall complexity of the algorithm can be reduced whereas the utilization of TPU on matrix multiplications is not compromised. However, this may sacrifice the capability of dealing with nonuniformly sampled data in the current implementation. Future work can also be done to improve the precision of matrix multiplications from float32 to float64. Another possibility of extending this work is to integrate the large-scale DFT on TPUs with the problems of medical image reconstruction, where a large number of iterations of nonuniform Fourier transform is often required in the optimization scheme. Finally, it is also possible to extend the implementation into a framework and address large-scale Fourier transform of higher dimensions.

VII. ACKNOWLEDGMENT

We would like to thank David Majnemer, Reid Tatge, Dehao Chen, Yusef Shafi, Damien Pierce, James Lottes, Matthias Ihme, and Rene Salmon for valuable discussions and helpful comments, which have greatly improved the paper.

REFERENCES

- [1] R. N. Bracewell and R. N. Bracewell, *The Fourier transform and its applications*. McGraw-Hill New York, 1986, vol. 31999.
- [2] A. Grama, V. Kumar, A. Gupta, and G. Karypis, *Introduction to parallel computing*. Pearson Education, 2003.
- [3] D. Takahashi, *Fast Fourier transform algorithms for parallel computers*. Springer, 2019.
- [4] R. Cont, *Frontiers in quantitative finance: Volatility and credit risk modeling*. John Wiley & Sons, 2009, vol. 519.
- [5] G. B. Giannakis, F. Bach, R. Cendrillon, M. Mahoney, and J. Neville, “Signal processing for big data [from the guest editors],” *IEEE Signal Processing Magazine*, vol. 31, no. 5, pp. 15–16, 2014.
- [6] E. Olshannikova, A. Ometov, Y. Koucheryavy, and T. Olsson, “Visualizing big data with augmented and virtual reality: challenges and research agenda,” *Journal of Big Data*, vol. 2, no. 1, p. 22, 2015.
- [7] J. W. Cooley and J. W. Tukey, “An algorithm for the machine calculation of complex Fourier series,” *Mathematics of computation*, vol. 19, no. 90, pp. 297–301, 1965.
- [8] P. Duhamel and H. Hollmann, “Split radix FFT algorithm,” *Electronics letters*, vol. 20, no. 1, pp. 14–16, 1984.
- [9] G. Ackins, “Fast fourier transform via ILLIAC IV,” *ILLIAC IV Document*, no. 146, 1968.
- [10] J. E. Stevens Jr *et al.*, “A fast Fourier transform subroutine for ILLIAC IV,” *CAC document*; no. 17, 1971.
- [11] P. N. Swartztrauber, “Multiprocessor FFTs,” *Parallel computing*, vol. 5, no. 1-2, pp. 197–210, 1987.
- [12] D. H. Bailey, “FFTs in external or hierarchical memory,” *The journal of Supercomputing*, vol. 4, no. 1, pp. 23–35, 1990.
- [13] A. Gupta and V. Kumar, “The scalability of FFT on parallel computers,” *IEEE Transactions on Parallel and Distributed Systems*, vol. 4, no. 8, pp. 922–932, 1993.
- [14] M. Frigo and S. G. Johnson, “The design and implementation of FFTW3,” *Proceedings of the IEEE*, vol. 93, no. 2, pp. 216–231, 2005.
- [15] D. Pekurovsky, “P3DFFT: A framework for parallel computations of Fourier transforms in three dimensions,” *SIAM Journal on Scientific Computing*, vol. 34, no. 4, pp. C192–C209, 2012.
- [16] D. Takahashi, “An implementation of parallel 3-D FFT with 2-D decomposition on a massively parallel cluster of multi-core processors,” in *International Conference on Parallel Processing and Applied Mathematics*. Springer, 2009, pp. 606–614.
- [17] D. T. Popovici, M. D. Schatz, F. Franchetti, and T. M. Low, “A flexible framework for parallel multi-dimensional DFTs,” *arXiv preprint arXiv:1904.10119*, 2019.
- [18] J. Kim. (2018) Leveraging optimized FFT on Intel Xeon platforms. [Online]. Available: <https://www.alcf.anl.gov/support-center/training-assets/leveraging-optimized-fft-intel-xeon-platforms>
- [19] K. R. Roe, K. Hester, and R. Pascual. (2019) Multi-GPU FFT performance on different hardware configurations. [Online]. Available: <https://developer.nvidia.com/gtc/2019/video/S9158>
- [20] D. Foley and J. Danskin, “Ultra-performance Pascal GPU and NVLink interconnect,” *IEEE Micro*, vol. 37, no. 2, pp. 7–17, Mar 2017.
- [21] A. Li, S. L. Song, J. Chen, J. Li, X. Liu, N. Tallent, and K. Barker, “Evaluating modern GPU interconnect: PCIe, NVLink, NV-SLI, NVSwitch and GPUDirect,” *arXiv preprint arXiv:1903.04611*, 2019.
- [22] Y. Chen, X. Cui, and H. Mei, “Large-scale FFT on GPU clusters,” in *Proceedings of the 24th ACM International Conference on Supercomputing*. ACM, 2010, pp. 315–324.
- [23] S. K. Nag and H. K. Verma, “Method for parallel-efficient configuring an FPGA for large FFTs and other vector rotation computations,” Feb. 1 2000, US Patent 6,021,423.
- [24] M. Garrido, M. Acevedo, A. Ehliar, and O. Gustafsson, “Challenging the limits of FFT performance on FPGAs,” in *2014 International Symposium on Integrated Circuits (ISIC)*. IEEE, 2014, pp. 172–175.
- [25] C.-L. Yu, K. Irick, C. Chakrabarti, and V. Narayanan, “Multidimensional DFT IP generator for FPGA platforms,” *IEEE Transactions on Circuits and Systems I: Regular Papers*, vol. 58, no. 4, pp. 755–764, 2010.
- [26] I. Stoica, D. Song, R. A. Popa, D. Patterson, M. W. Mahoney, R. Katz, A. D. Joseph, M. Jordan, J. M. Hellerstein, J. E. Gonzalez *et al.*, “A Berkeley view of systems challenges for AI,” *arXiv preprint arXiv:1712.05855*, 2017.
- [27] N. P. Jouppi, C. Young, N. Patil, D. Patterson, G. Agrawal, R. Bajwa, S. Bates, S. Bhatia, N. Boden, A. Borchers *et al.*, “In-datacenter performance analysis of a tensor processing unit,” in *2017 ACM/IEEE 44th Annual International Symposium on Computer Architecture (ISCA)*. IEEE, 2017, pp. 1–12.
- [28] Cloud TPUs. [Online]. Available: <https://cloud.google.com/tpu/>

- [29] N. Jouppi. (2017) Quantifying the performance of the TPU, our first machine learning chip. [Online]. Available: <https://cloud.google.com/blog/products/gcp/quantifying-the-performance-of-the-tpu-our-first-machine-learning-chip>
- [30] Y. Wu, M. Schuster, Z. Chen, Q. V. Le, M. Norouzi, W. Macherey, M. Krikun, Y. Cao, Q. Gao, K. Macherey *et al.*, “Google’s neural machine translation system: Bridging the gap between human and machine translation,” *arXiv preprint arXiv:1609.08144*, 2016.
- [31] N. Ketkar, “Introduction to PyTorch,” in *Deep learning with Python*. Springer, 2017, pp. 195–208.
- [32] K. Yang, Y.-F. Chen, G. Roumpos, C. Colby, and J. Anderson, “High performance Monte Carlo simulation of Ising model on TPU clusters,” in *Proceedings of the International Conference for High Performance Computing, Networking, Storage and Analysis*, ser. SC ’19. ACM, 2019, pp. 83:1–83:15. [Online]. Available: <http://doi.acm.org/10.1145/3295500.3356149>
- [33] F. Belletti, D. King, K. Yang, R. Nelet, Y. Shafi, Y.-F. Chen, and J. Anderson, “Tensor processing units for financial Monte Carlo,” *arXiv preprint arXiv:1906.02818*, 2019.
- [34] S. Bagchi and S. K. Mitra, “The nonuniform discrete Fourier transform and its applications in filter design. I. 1-D;” *IEEE Transactions on Circuits and Systems II: Analog and Digital Signal Processing*, vol. 43, no. 6, pp. 422–433, 1996.
- [35] —, “The nonuniform discrete Fourier transform and its applications in filter design. II. 2-D;” *IEEE Transactions on Circuits and Systems II: Analog and Digital Signal Processing*, vol. 43, no. 6, pp. 434–444, 1996.
- [36] J.-Y. Lee and L. Greengard, “The type 3 nonuniform FFT and its applications,” *Journal of Computational Physics*, vol. 206, no. 1, pp. 1–5, 2005.
- [37] A. Rahimi and B. Recht, “Random features for large-scale kernel machines,” in *Advances in neural information processing systems*, 2008, pp. 1177–1184.
- [38] Using bfloat16 with TensorFlow models. [Online]. Available: <https://cloud.google.com/tpu/docs/bfloat16>
- [39] G. Henry, P. T. P. Tang, and A. Heinecke, “Leveraging the bfloat16 artificial intelligence datatype for higher-precision computations,” *arXiv preprint arXiv:1904.06376*, 2019.
- [40] P. A. Regalia and M. K. Sanjit, “Kronecker products, unitary matrices and signal processing applications,” *SIAM review*, vol. 31, no. 4, pp. 586–613, 1989.